flashes at opposite edges of the computer screen (see Supplementary Information).

We also investigated the possibility that the offset-matched flash appears brighter (or perhaps more salient) because attention shifts to it. However, attention shifts are slow ($\sim$200–300 ms, ref. 8), whereas the brief flash appears and disappears within 56 ms. None-theless, we manipulated the contrast polarity of the background to test the attentional explanation. When the background was brighter than the flashes, the offset-matched brief flash appeared dimmer, not brighter, than the onset-matched flash (Fig. 2d; $t = -2.2$, $P = 0.026$). More importantly, when the background and flashes were made equiluminant, observers perceived no significant bright-ness illusion, arguing against a salience-enhancing attentional shift (Fig. 2d; $t = -0.58$, $P = 0.28$).

Spatial interactions in brightness perception are well known[1,2] but provide an incomplete description; the TCE shows that bright-ness is influenced by temporal context as well. Our results further show a surprising juxtaposition of facts: first, that information encoded about the brightness of stimuli changes over time, such that the appearance of physically identical brief flashes compared to a persisting long flash varies as a function of stimulus onset asynchrony (Fig. 1c); and yet, second, the perceived brightness of a long flash remains constant over time (Fig. 2a). This indicates that brightness encoding might involve at least two neural populations: one with an adapting response that diminishes over time, and the other with a downstream response that assigns brightness labels to objects and does not adapt. We propose that the TCE arises from an interaction between these non-adapting and adapting encodings. In our model, activity in the non-adapting population remains con-stant—thereby encoding an unchanging label—even while its input from the adapting population diminishes (Supplementary Fig. S1; for an example of such hysteresis, see ref. 9). The hypothesis that some neurons maintain a brightness label is consistent with the idea that the brain strives to monitor the external world undistracted by predictable changes in its own physiology.

The activity of some neurons in primary visual cortex is corre-lated with brightness; that is, the firing rate varies as a function of surrounding luminance, even as the luminance in the receptive field remains unchanged[10–14]. The activity of these brightness-responsive neurons adapts with time: the firing rates peak after 100 ms and then drop off precipitously[14]. This decrease in firing is consistent with an adapting population, although in some circumstances the later part of the spike train may correspond to the response of a non-adapting population[14]. This raises the possibility that the two encodings could be multiplexed into the same population of cells in V1. The TCE separates the physical measure of luminance and the percep-tual quality of brightness (which typically co-vary) and offers a new approach for examining the neural coding of brightness. □

1. Gilchrist, A. *Lightness, Brightness and Transparency* (Lawrence Erlbaum Associates, Hillsdale, New Jersey, 1994).
2. Eagleman, D. M. Visual illusions and neurobiology. *Nature Rev. Neurosci.* **2**, 920–926 (2001).
3. Koffka, K. *Principles of Gestalt Psychology* (Harcourt, Brace, and World, New York, 1935).
4. Knill, D. C. & Kersten, D. Apparent surface curvature affects lightness perception. *Nature* **351**, 228–230 (1991).
5. Adelson, E. H. Perceptual organization and the judgment of brightness. *Science* **262**, 2042–2044 (1993).
6. Gilchrist, A. L. Lightness contrast and failures of constancy: a common explanation. *Percept. Psychophys.* **43**, 415–424 (1988).
7. Broca, A. & Sulzer, D. La sensation lumineuse en fonction du temps. *J. Physiol. Pathol. Gén.* **4**, 632–640 (1902).
8. Weichselgartner, E. & Sperling, G. Dynamics of automatic and controlled visual attention. *Science* **238**, 778–780 (1987).
9. Hahnloser, R. H., Sarpeshkar, R., Mahowald, M. A., Douglas, R. J. & Seung, H. S. Digital selection and analogue amplification coexist in a cortex-inspired silicon circuit. *Nature* **405**, 947–951 (2000).
10. Rossi, A. F. & Paradiso, M. A. Neural correlates of perceived brightness in the retina, lateral geniculate nucleus, and striate cortex. *J. Neurosci.* **19**, 6145–6156 (1999).
11. Rossi, A. F., Rittenhouse, C. D. & Paradiso, M. A. The representation of brightness in primary visual cortex. *Science* **273**, 1104–1107 (1996).
12. MacEvoy, S. P., Kim, W. & Paradiso, M. A. Integration of surface information in primary visual cortex. *Nature Neurosci.* **1**, 616–620 (1998).
13. Hung, C. P., Ramsden, B. M., Chen, L. M. & Roe, A. W. Building surfaces from borders in Areas 17 and 18 of the cat. *Vision Res.* **41**, 1389–1407 (2001).
14. Kinoshita, M. & Komatsu, H. Neural representation of the luminance and brightness of a uniform surface in the macaque primary visual cortex. *J. Neurophysiol.* **86**, 2559–2570 (2001).
15. Bowen, R. W., Pokorny, J. & Smith, V. C. Sawtooth contrast sensitivity: decrements have the edge. *Vision Res.* **29**, 1501–1509 (1989).
16. Cowey, A. & Rolls, E. T. Human cortical magnification factor and its relation to visual acuity. *Exp. Brain Res.* **21**, 447–454 (1974).

Integration of quanta in cerebellar granule cells during sensory processing

Paul Chadderton, Troy W. Margie & Michael Häusser

Wolfson Institute for Biomedical Research and Department of Physiology, University College London, Gower Street, London WC1E 6BT, UK

To understand the computations performed by the input layers of cortical structures, it is essential to determine the relationship between sensory-evoked synaptic input and the resulting pattern of output spikes. In the cerebellum, granule cells constitute the input layer, translating mossy fibre signals into parallel fibre input to Purkinje cells[1]. Until now, their small size and dense packing[1,2] have precluded recordings from individual granule cells *in vivo*. Here we use whole-cell patch-clamp recordings to show the relationship between mossy fibre synaptic currents evoked by somatosensory stimulation and the resulting granule cell output patterns. Granule cells exhibited a low ongoing firing rate, due in part to dampening of excitability by a tonic inhibi-tory conductance mediated by GABA$_A$ (γ-aminobutyric acid type A) receptors. Sensory stimulation produced bursts of mossy fibre excitatory postsynaptic currents (EPSCs) that summate to trigger bursts of spikes. Notably, these spike bursts were evoked by only a few quantal EPSCs, and yet spontaneous mossy fibre inputs triggered spikes only when inhibition was reduced. Our results reveal that the input layer of the cerebellum balances exquisite sensitivity with a high signal-to-noise ratio. Granule cell bursts are optimally suited to trigger glutamate receptor activation[3–5] and plasticity[6–8] at parallel fibre synapses, providing a link between input representation and memory storage in the cerebellum.

Cerebellar granule cells are the smallest and most numerous neurons in the mammalian brain and have a simple morphology with an average of only four short dendrites[1,2], each dendrite receiving a single excitatory mossy fibre input. Each granule cell also receives inhibitory input from one or two Golgi cells[1,2], the major granular layer interneuron (Fig. 1a). The combination of such a small number of inputs to an electrotonically compact structure[9,10] provides an ideal model in which to study synaptic
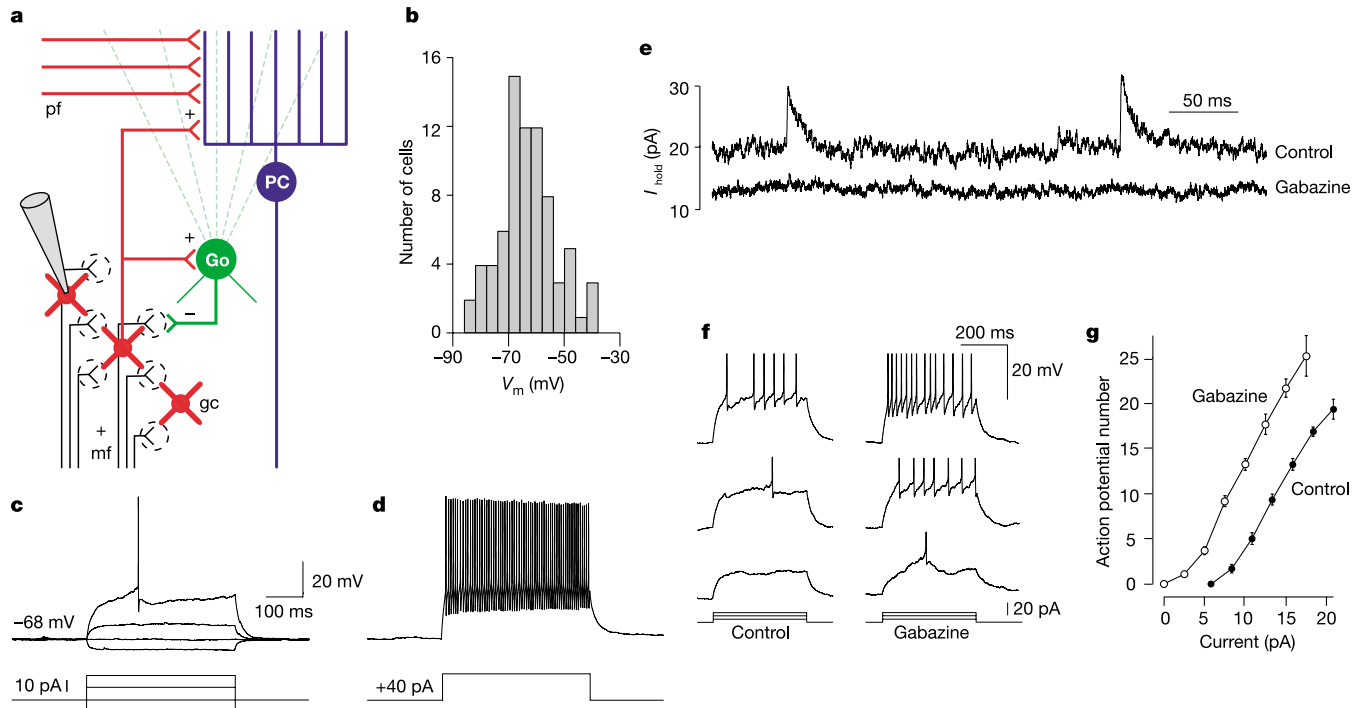
Figure 1 Intrinsic membrane properties of granule cells *in vivo*. **a**, Schematic diagram showing the basic connectivity in the cerebellar granule cell layer (mf, mossy fibre; gc, granule cell; pf, parallel fibre; PC, Purkinje cell; Go, Golgi cell). **b**, Histogram of granule cell resting membrane potentials (V_m; ketamine/xylazine or urethane anaesthesia). **c**, **d**, Responses to current injection at resting potential show inward rectification and non-accommodating spikes at up to 250 Hz (urethane anaesthesia). **e**, Voltage-clamp recording at 0 mV. Gabazine (0.5 mM) abolished outward currents and reduced the tonic holding current. **f**, Responses to current injection before and after gabazine application (action potentials truncated). **g**, Increased excitability in gabazine is reflected in a leftward shift of the *f–I* curve.

integration *in vivo*. To investigate input–output transformations during sensory activation, we made whole-cell patch-clamp recordings from granule cells in crus I and IIa of the cerebellar cortex, regions that produce strong multiunit and field responses during tactile stimulation of the vibrissae and the lip area in anaesthetized rats[11–13]. Granule cells were identified by their depth ($>400\,\mu m$ from the pial surface) and their characteristic electrophysiological properties (high input resistance ($1.1 \pm 0.1\,G\Omega$ at rest, $n = 62$ cells), small capacitance ($\leq 5\,pF$) and fast membrane time constant ($\tau = 6.9 \pm 0.7\,ms$, $n = 49$; refs 9, 14, 15)). Granule cells exhibited a resting membrane potential of $-64 \pm 1\,mV$ ($24 \pm 1\,mV$ hyperpolarized to threshold, $n = 75$; Fig. 1b) and strong inward rectification (Fig. 1c), with input resistance nearly doubling when depolarizing from -75 to $-50\,mV$ (ratio 1.9 ± 0.1, $n = 17$). Firing frequencies of up to 250 Hz were observed with little or no accommodation (accommodation ratio $= 0.9 \pm 0.1$, $n = 11$) in response to strong depolarizing current pulses (Fig. 1d). These properties are consistent with those described for granule cells *in vitro*[14–17].

Granule cells exhibited a low firing rate *in vivo*, with the mean spontaneous firing rate in the absence of holding current being $0.5 \pm 0.2\,Hz$ ($n = 46$). This low firing rate may reflect low excitatory drive or strong inhibition. To investigate synaptic input to granule cells *in vivo*, voltage-clamp recordings were made at -70 or $0\,mV$ (the reversal potentials for GABA$_A$ and AMPA (α-amino-3-hydroxy-5-methyl-4-isoxazole propionic acid) receptor-mediated currents, respectively). At $-70\,mV$, spontaneous EPSCs sensitive to the AMPA receptor antagonist NBQX were recorded at a frequency of $4 \pm 1\,Hz$ (amplitude $-8.7 \pm 1.1\,pA$, $n = 10$). At $0\,mV$, spontaneous inhibitory postsynaptic currents (IPSCs) sensitive to the selective GABA$_A$ receptor blocker gabazine (SR95531) were observed at a frequency of $5 \pm 1\,Hz$ (amplitude $= 9.6 \pm 2.7\,pA$, $n = 10$). In addition to blocking IPSCs (Fig. 1e), gabazine also
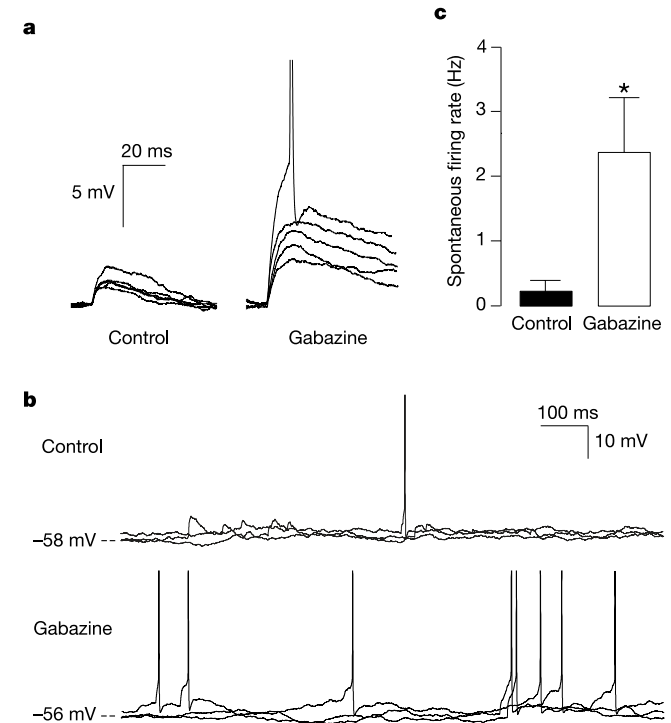

Figure 2 Low spontaneous firing rates are enforced by tonic inhibition *in vivo*. **a**, Representative spontaneous EPSPs before and after GABA$_A$ receptor blockade (action potential is truncated). EPSP amplitudes were increased in the presence of gabazine ($1.9 \pm 0.4\,mV$ to $3.7 \pm 0.5\,mV$, $P < 0.02$, $n = 4$). **b**, Current-clamp recording (three overlaid traces) from a granule cell at rest (top) and after GABA$_A$ receptor blockade (bottom). **c**, Spontaneous firing rates increased in the presence of gabazine (asterisk, $P < 0.05$, $n = 5$).

©2004 **Nature Publishing Group**

produced a significant reduction in the baseline holding current ($P < 0.001$, $n = 11$), an increase in input resistance measured at -60 mV (1.3 ± 0.5 to 2.5 ± 0.4 GΩ, $P < 0.01$, $n = 6$) and a depolarization of resting potential (3.8 ± 1.4 mV, $P < 0.05$, $n = 7$). This indicates that a tonic GABA$_A$ receptor-mediated conductance[15,16,18,19], due to persistent activation of extrasynaptic high-affinity GABA receptors[15,20], is present *in vivo*. This conductance had a powerful impact on the input–output function of granule cells *in vivo*, with gabazine producing a significant shift in the spike frequency–current (f–I) relationship ($P < 0.01$, $n = 3$; Fig. 1f, g) and increasing spontaneous mossy fibre excitatory postsynaptic potential (EPSP) amplitudes ($P < 0.02$, $n = 4$; Fig. 2a). As a consequence, during blocking of tonic inhibition, single EPSPs were on occasion capable of triggering action potentials (Fig. 2a; $n = 4$), with spontaneous firing rate increasing by an order of magnitude (Fig. 2b, c). Thus, spontaneous mossy fibre input is normally insufficient to trigger spike output owing in part to dampening of excitability by tonic inhibition. However, when tonic inhibition is reduced, unitary inputs are capable of driving granule cell output.

The input–output relationship of granule cells in response to physiologically relevant stimuli is unknown. We used air-puff stimulation of the vibrissae (or other facial regions; for example, upper lip) to evoke mossy fibre input to granule cells[11–13]. Sensory stimulation evoked excitatory responses in 14 granule cells (only

one of which demonstrated both evoked EPSCs and IPSCs). The latency of EPSCs from the onset of the stimulus was 40 ± 6 ms (range = 9–75 ms, $n = 10$), consistent with a predominantly corticopontine origin of evoked mossy fibre activity[13]. Evoked EPSCs usually occurred in high-frequency bursts (defined as synaptic events with intercurrent intervals <50 ms; average 3.2 ± 0.5 EPSCs at 75 ± 19 Hz, $n = 10$; see Fig. 3a, c, e). EPSCs within the burst were highly irregular (coefficient of variation of evoked EPSC intervals = 0.82 ± 0.07, $n = 5$). Sensory stimulation produced action potentials in seven out of ten whole-cell recordings where evoked responses were observed, with the most common discharge pattern consisting of a burst of several action potentials (3.3 ± 0.2 action potentials, $n = 7$, including two cell-attached recordings; Fig. 3b, d, f). The mean frequency of action potentials within evoked bursts was 77 ± 12 Hz, with maximal instantaneous frequencies being as high as 250 Hz (mean = 163 ± 19 Hz, $n = 7$). Changing stimulus duration did not significantly affect the pattern of bursting responses (action potential number, $F_{(3,136)} = 2.3$, $P > 0.05$; action potential frequency, $F_{(3,97)} = 0.6$, $P > 0.05$; one-way analysis of variance, $n = 3$ cells for 30–300 ms duration).

To investigate the origin of individual evoked currents, we compared the amplitudes of spontaneous EPSCs, which presumably reflect release from single mossy fibre boutons, with those evoked by sensory stimulation. The similarity in amplitude distributions of these two populations of EPSCs (Fig. 4a, b; mean -8.9 ± 1.0 pA
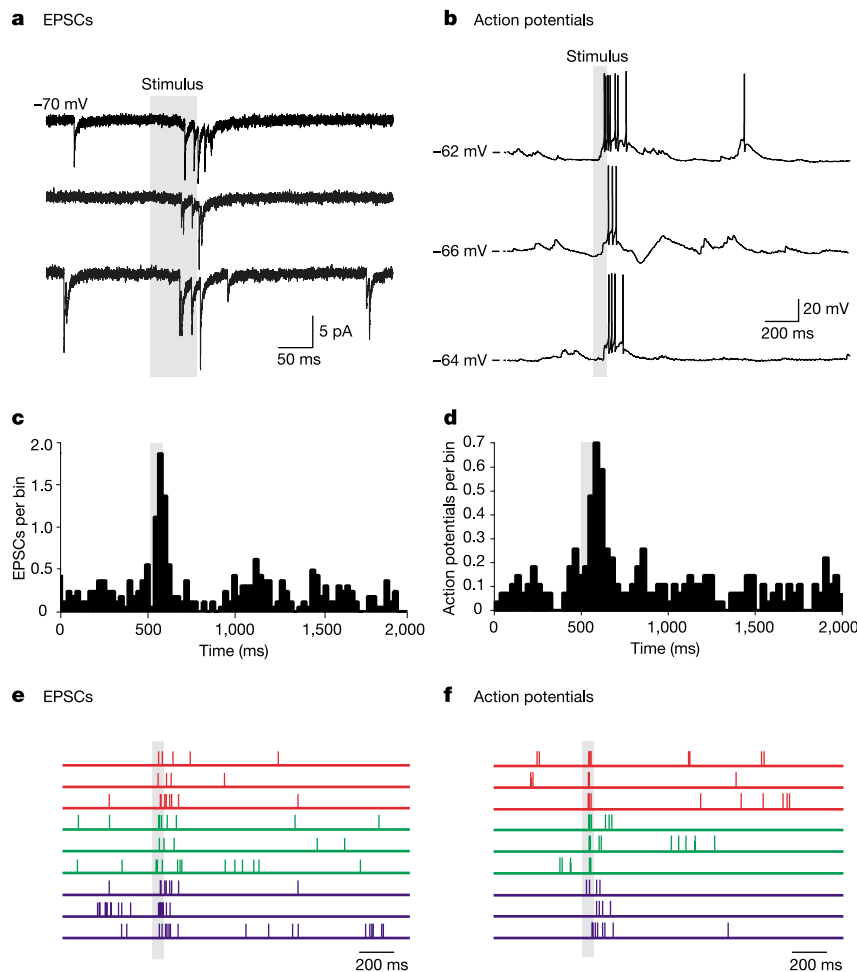

Figure 3 Evoked sensory responses in granule cells *in vivo*. **a**, EPSCs evoked by whisker stimulation recorded in voltage clamp at -70 mV (three consecutive trials). **b**, Action potentials evoked in response to whisker stimulation (three consecutive trials). **c**, **d**, Representative peristimulus time histogram of sensory-evoked EPSCs (**c**, 16 trials)

and action potentials (**d**, 16 trials) for individual granule cells. **e**, Raster plot of evoked EPSCs (three trials from three different granule cells, where each colour corresponds to a different cell). **f**, Raster plot of evoked action potentials (three trials from three different granule cells, with colours corresponding to the same cells as in **e**).

and -7.9 ± 0.6 pA at -70 mV for spontaneous and evoked EPSCs, respectively; $P = 0.28$, Kolmogorov–Smirnov test) indicates that individual evoked EPSCs originate from a single mossy fibre, with evoked EPSC bursts resulting from either a burst in a single presynaptic mossy fibre[21,22] or asynchronous activation of multiple mossy fibres. To determine the contribution of single quanta, we isolated miniature EPSCs by applying tetrodotoxin (TTX). Remarkably, this did not significantly change the amplitude distribution of EPSCs compared to control (Fig. 4c, d; mean amplitudes -8.6 ± 0.4 pA and -8.1 ± 0.3 pA for spontaneous and miniature EPSCs, respectively; $n = 4$, $P = 0.77$, Kolmogorov–Smirnov test). The similarity of miniature spontaneous and evoked EPSCs indicates that release probability at mossy fibre synapses is likely to be low, and that sensory stimulation evokes bursts of EPSCs that each are composed of only one or two quanta.

To explore the link between the bursting pattern of mossy fibre EPSC inputs and bursting output, we compared spiking responses to different temporal patterns of EPSC waveforms injected into the granule cell *in vivo*. A burst of three EPSCs at 80 Hz produced a burst of action potentials that could not be evoked by a single EPSC with the same charge integral (2.9 ± 0.2 versus 1.5 ± 0.3 action potentials, respectively, $P < 0.001$, unpaired *t*-test, $n = 4$; Supplementary Fig. 1). This provides direct evidence that the tem-

porally distributed pattern of input promotes burst firing in granule cells. Burst firing will be enhanced further by the nonlinear properties of synaptic integration exhibited by granule cells, which include NMDA receptor and persistent sodium channel activation[14,17]. Nonlinearities also contribute to integration *in vivo*, with depolarization from -60 mV to -50 mV producing a 1.6-fold increase in the integral of spontaneous EPSPs ($P < 0.05$, $n = 8$; Supplementary Fig. 2).

In a few granule cells, we were able to record both evoked EPSCs and action potentials in the same cells, allowing us to directly relate mossy fibre input to action potential output (Fig. 4e; $n = 5$). These experiments demonstrate that the number of output action potentials is intimately linked to the number of input EPSCs. On average, the EPSC/action potential relationship falls below the unity line, indicating that EPSP summation is required to generate spiking. This could be observed directly in some experiments, where action potentials usually occurred only after summation of two or more EPSPs (Fig. 4f).

We have taken advantage of the highly favourable anatomical and physiological properties of the cerebellar granule cell to investigate directly single-cell input–output computations in a cortical input layer *in vivo*. Our findings provide the first direct evidence in support of theoretical predictions that the spontaneous firing rate of granule cells *in vivo* is low, which will increase the number of distinct patterns of input that can be represented by the cerebellar cortex[23,24]. Low firing rates are ensured by a hyperpolarized membrane potential and a tonic GABAergic conductance. We show that this conductance regulates the transformation of mossy fibre input into granule cell output, such that when tonic inhibition is reduced (as may occur after nitric oxide release[25] or changes in steroid levels[20]), information arriving via a single mossy fibre action potential can be transferred through the granule cell layer. This is a critical requirement if the network is to remain sensitive to low levels of afferent activity[23].

Our finding that bursts of action potentials in granule cells are triggered by clustered sensory-evoked mossy fibre EPSCs complements and enhances existing theories of cerebellar function[23,24] that propose that the granule cell layer is a low-noise sparse coding system. This burst-to-burst sequence ensures that granule cells reliably relay sensory-evoked mossy fibre signals, whereas events not associated with sensory stimulation are filtered out. Bursting thus further enhances the signal-to-noise ratio for transfer of sensory information in an input layer exhibiting low firing rates[26–29]. We demonstrate that the bursting pattern of granule cell discharge is due to temporally distributed synaptic input. Notably, these clusters of EPSCs are composed of only a small number of quanta, indicating that granule cells are highly sensitive to individual quanta when they are temporally correlated by sensory input. This relay can therefore approach maximal sensitivity (that is, one quantum) depending on tonic inhibition and levels of mossy fibre input[23].

Bursts in granule cells have special relevance for the cerebellar network, as the downstream synapses made onto Purkinje cells show frequency-dependent facilitation of transmitter release[3,5] and glutamate receptor activation[4], suggesting that granule cell bursting will be nonlinearly amplified at the next synaptic relay[27]. This will enhance postsynaptic activation of Purkinje cells through both ascending branch[30] and parallel fibre synapses, with the duration of the burst offering a relatively broad window for postsynaptic coincidence detection. Because induction of synaptic plasticity at these synapses is also highly frequency-dependent[6–8], granule cell bursting may provide a substrate for the storage of sensory representations. □
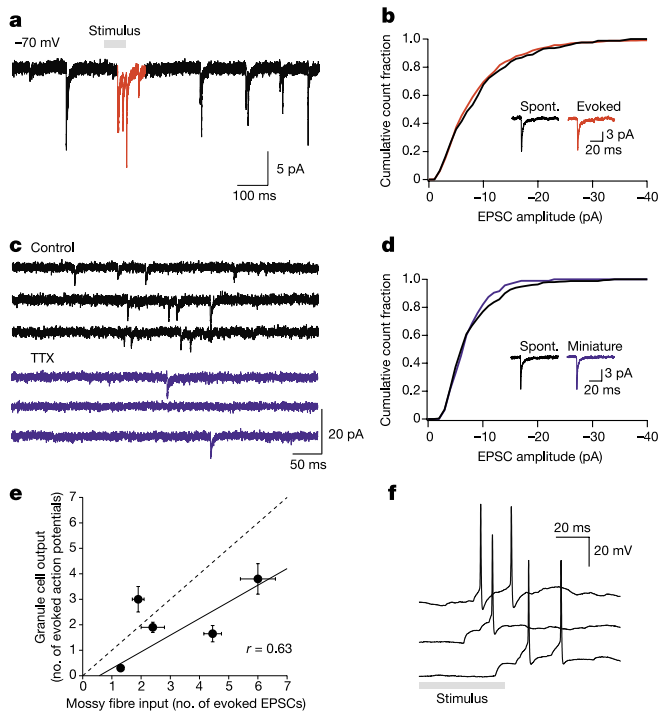

Figure 4 The relationship between mossy fibre input and granule cell output. **a**, Representative sensory-evoked EPSCs (red). **b**, Normalized cumulative amplitude histogram for spontaneous and evoked EPSCs ($n = 4$ cells; 1 pA bins). Inset: average EPSCs from a single cell. **c**, Spontaneous EPSCs and miniature EPSCs after TTX application. **d**, Normalized cumulative amplitude histogram for spontaneous and miniature EPSCs ($n = 5$, 1 pA bins). Inset: average EPSCs from a single cell. **e**, The relationship between the number of evoked mossy fibre EPSCs and granule cell action potentials at resting potential (-55 ± 5 mV). Each point represents a single granule cell. The dashed line indicates when the EPSC/action potential ratio equals one. Cells below this line (4 out of 5) require EPSP summation in order to generate output. The solid line is a linear fit to data points weighted by s.e.m. **f**, Representative traces showing summation of evoked EPSPs and resulting action potentials. In 86% of trials, at least two sensory-evoked EPSPs were required to summate to produce the first action potential in the response.

Methods

letters to nature

clamp and voltage-clamp recordings were made using a Multiclamp 700A amplifier (Axon Instruments). Patch pipettes (4–8 MΩ) were filled with a K-methanesulphonate-based internal solution (7 mM Cl⁻). Sensory responses were evoked by an air puff (30–300 ms, 60 p.s.i.) timed by a Picospritzer (General Valve) and delivered to the ipsilateral perioral surface. Data are represented as mean ± s.e.m. See Supplementary Methods for further details.

1. Eccles, J. C., Ito, M. & Szentagothai, J. *The Cerebellum as a Neuronal Machine* (Springer, Berlin, 1967).
2. Jakab, R. L. & Hamori, J. Quantitative morphology and synaptology of cerebellar glomeruli in the rat. *Anat. Embryol. (Berl.)* **179**, 81–88 (1988).
3. Konnerth, A., Llano, I. & Armstrong, C. M. Synaptic currents in cerebellar Purkinje cells. *Proc. Natl Acad. Sci. USA* **87**, 2662–2665 (1990).
4. Takechi, H., Eilers, J. & Konnerth, A. A new class of synaptic response involving calcium release in dendritic spines. *Nature* **396**, 757–760 (1998).
5. Perkel, D. J., Hestrin, S., Sah, P. & Nicoll, R. A. Excitatory synaptic currents in Purkinje cells. *Proc. R. Soc. Lond. B* **241**, 116–121 (1990).
6. Casado, M., Isope, P. & Ascher, P. Involvement of presynaptic N-methyl-D-aspartate receptors in cerebellar long-term depression. *Neuron* **33**, 123–130 (2002).
7. Wang, S. S.-H., Denk, W. & Häusser, M. Coincidence detection in single dendritic spines mediated by calcium release. *Nature Neurosci.* **3**, 1266–1273 (2000).
8. Brown, S. P., Brenowitz, S. D. & Regehr, W. G. Brief presynaptic bursts evoke synapse-specific retrograde inhibition mediated by endogenous cannabinoids. *Nature Neurosci.* **6**, 1048–1057 (2003).
9. Silver, R. A., Traynelis, S. F. & Cull-Candy, S. G. Rapid-time-course miniature and evoked excitatory currents at cerebellar synapses *in situ. Nature* **355**, 163–166 (1992).
10. Gabbiani, F., Midtgaard, J. & Knöpfel, T. Synaptic integration in a model of cerebellar granule cells. *J. Neurophysiol.* **72**, 999–1009 (1994).
11. Shambes, G. M., Gibson, J. M. & Welker, W. Fractured somatotopy in granule cell tactile areas of rat cerebellar hemispheres revealed by micromapping. *Brain Behav. Evol.* **15**, 94–140 (1978).
12. Bower, J. M. & Woolston, D. C. Congruence of spatial organization of tactile projections to granule cell and Purkinje cell layers of cerebellar hemispheres of the albino rat: vertical organization of cerebellar cortex. *J. Neurophysiol.* **49**, 745–766 (1983).
13. Morissette, J. & Bower, J. M. Contribution of somatosensory cortex to responses in the rat cerebellar granule cell layer following peripheral tactile stimulation. *Exp. Brain Res.* **109**, 240–250 (1996).
14. D'Angelo, E., De Filippi, G., Rossi, P. & Taglietti, V. Synaptic excitation of individual rat cerebellar granule cells *in situ*: evidence for the role of NMDA receptors. *J. Physiol. (Lond.)* **484**, 397–413 (1995).
15. Brickley, S. G., Revilla, V., Cull-Candy, S. G., Wisden, W. & Farrant, M. Adaptive regulation of neuronal excitability by a voltage-independent potassium conductance. *Nature* **409**, 88–92 (2001).
16. Brickley, S. G., Cull-Candy, S. G. & Farrant, M. Development of a tonic form of synaptic inhibition in rat cerebellar granule cells resulting from persistent activation of GABA_A receptors. *J. Physiol. (Lond.)* **497**, 753–759 (1996).
17. D'Angelo, E., De Filippi, G., Rossi, P. & Taglietti, V. Ionic mechanism of electroresponsiveness in cerebellar granule cells implicates the action of a persistent sodium current. *J. Neurophysiol.* **80**, 493–503 (1998).
18. Wall, M. J. & Usowicz, M. M. Development of action potential-dependent and independent spontaneous GABA_A receptor-mediated currents in granule cells of postnatal rat cerebellum. *Eur. J. Neurosci.* **9**, 533–548 (1997).
19. Hamann, M., Rossi, D. J. & Attwell, D. Tonic and spillover inhibition of granule cells control information flow through cerebellar cortex. *Neuron* **33**, 625–633 (2002).
20. Stell, B. M., Brickley, S. G., Tang, C. Y., Farrant, M. & Mody, I. Neuroactive steroids reduce neuronal excitability by selectively enhancing tonic inhibition mediated by δ subunit-containing GABA_A receptors. *Proc. Natl Acad. Sci. USA* **100**, 14439–14444 (2003).
21. Eccles, J. C., Faber, D. S., Murphy, J. T., Sabah, N. H. & Taborikova, H. Afferent volleys in limb nerves influencing impulse discharges in cerebellar cortex. I. In mossy fibers and granule cells. *Exp. Brain Res.* **13**, 15–35 (1971).
22. Garwicz, M., Jörntell, H. & Ekerot, C. F. Cutaneous receptive fields and topography of mossy fibres and climbing fibres projecting to cat cerebellar C3 zone. *J. Physiol. (Lond.)* **512**, 277–293 (1998).
23. Marr, D. A theory of cerebellar cortex. *J. Physiol. (Lond.)* **202**, 437–470 (1969).
24. Albus, J. S. A theory of cerebellar function. *Math. Biosci.* **10**, 25–61 (1971).
25. Wall, M. J. Endogenous nitric oxide modulates GABAergic transmission to granule cells in adult rat cerebellum. *Eur. J. Neurosci.* **18**, 869–878 (2003).
26. Krahe, R. & Gabbiani, F. Burst firing in sensory systems. *Nature Rev. Neurosci.* **5**, 13–23 (2004).
27. Lisman, J. E. Bursts as a unit of neural information: making unreliable synapses reliable. *Trends Neurosci.* **20**, 38–43 (1997).
28. Hahnloser, R. H., Kozhevnikov, A. A. & Fee, M. S. An ultra-sparse code underlies the generation of neural sequences in a songbird. *Nature* **419**, 65–70 (2002).
29. Margrie, T. W., Brecht, M. & Sakmann, B. *In vivo*, low-resistance, whole-cell recordings from neurons in the anaesthetized and awake mammalian brain. *Pflügers Arch.* **444**, 491–498 (2002).
30. Llinás, R. in *The Cerebellum: New Vistas* (eds Palay, S. L. & Chan-Palay, V.) 189–194 (Springer, New York, 1982).

Birth of parthenogenetic mice that can develop to adulthood

Tomohiro Kono[1,3], Yayoi Obata[1,3], Quiong Wu[1,3], Katsutoshi Niwa[1,3], Yukiko Ono[1], Yuji Yamamoto[2,3], Eun Sung Park[4], Jeong-Sun Seo[4,5] & Hidehiko Ogawa[1,3]

[1]Department of BioScience, and [2]Department of Applied Science, Tokyo University of Agriculture, Setagaya-ku, Tokyo 156-8502, Japan
[3]Bio-oriented Technology Research Advancement Institution (BRAIN), Minato-ku, Tokyo 105-0001, Japan
[4]MacroGen Inc, Chongno-Ku, Seoul 110-061, Korea
[5]Department of Biochemistry, Seoul National University College of Medicine, Chongno-Ku, Seoul 110-799, Korea

Only mammals have relinquished parthenogenesis, a means of producing descendants solely from maternal germ cells. Mouse parthenogenetic embryos die by day 10 of gestation[1–4]. Bi-parental reproduction is necessary because of parent-specific epigenetic modification of the genome during gametogenesis[5–8]. This leads to unequal expression of imprinted genes from the maternal and paternal alleles[9]. However, there is no direct evidence that genomic imprinting is the only barrier to parthenogenetic development. Here we show the development of a viable parthenogenetic mouse individual from a reconstructed oocyte containing two haploid sets of maternal genome, derived from non-growing and fully grown oocytes. This development was made possible by the appropriate expression of the *Igf2* and *H19* genes with other imprinted genes, using mutant mice with a 13-kilobase deletion in the *H19* gene[10] as non-growing oocytes donors. This full-term development is associated with a marked reduction in aberrantly expressed genes. The parthenote developed to adulthood with the ability to reproduce offspring. These results suggest that paternal imprinting prevents parthenogenesis, ensuring that the paternal contribution is obligatory for the descendant.

Maternal-specific *de novo* methylation of imprinted loci occurs during oocyte growth[7,8,11,12]; such non-growing oocytes from new-born mice are considered to be naive with respect to most of the maternal imprinting process. Parthenogenetic mouse embryos (ng^wt/fg^wt) that contain genomes from non-growing (ng^wt) and fully grown (fg^wt) oocytes can develop into 13.5-day-old fetuses[12], by the appropriate expression of many imprinted genes[13]. However, the imprinted expression of the *H19* and *Igf2* genes has not been altered in the ng allele. The expression of the *Igf2* and *H19* genes are coordinately regulated by *cis*-acting elements, depending on the methylation status of the differentially methylated region (DMR) of the *H19* gene[14–16] and on endoderm-specific enhancers[17] (Fig. 1i). To block *H19* gene expression from ng oocyte alleles, mutant mice harbouring a 3-kilobase (kb) deletion in the *H19* transcription unit[18] were used to construct parthenogenetic embryos. The ng^{H19Δ3}/fg^wt parthenotes developed as live fetuses for 17.5 days of gestation, but showed no sign of further development[19]. The *Igf2*

Table 1 Development of reconstructed parthenogenetic embryos

Developmental progress	Number
Number of reconstructed eggs	457
Number of embryos developed to blastocysts	417 (91.2% of reconstructed eggs)
Number of embryos transferred	371 (89.0% of blastocysts)
Number pregnants/recipients	24/26
Number of implantation to recipients	246 (71.7% of embryos transferred to pregnants)
Number of pups	28 (8.2% of embryos transferred to pregnants)
Dead	18 (5.2% of embryos transferred to pregnants)
Live	8 (2.3% of embryos transferred to pregnants)
Survived	2 (0.6% of embryos transferred to pregnants)